Global Research journal of Natural Science and Technology (Grjnst)
Volume: 03 - Issue 4 (2024)
p.ISSN: 2790-7643 e.ISSN: 2790-7651
www.grjnst.com

Visible-Light-Driven Photocatalytic Degradation of Methylene Blue by a Magnetically Recoverable Fe-Cu@rGO Nano composite: Mechanistic Insights and Thermodynamic Analysis

Alishba Gull
Faculty of Sciences, Superior University Lahore, Lahore 54000, Pakistan
Kainat Arshad
Institute of Chemistry, University of Sargodha, Sargodha 40100, Pakistan

Muhammad Ashraf Shaheen (Corresponding Author)
Faculty of Sciences, Superior University Lahore, Lahore 54000, Pakistan
Email: masaheen1964@gmail.com

Muhammad Azhar Abbas
Institute of Chemistry, University of Sargodha, Sargodha 40100, Pakistan/ Government Ambala Muslim Graduate College, Sargodha 40100, Pakistan

Abstract

The production of effective, durable as well as regenerative photocatalysts is crucial to achieving sustainable remediation of water. In this work, the authors provide application-based research on a pre-synthesized bimetallic iron-copper decorated reduced graphene oxide nanocomposite (Fe-Cu@rGO) to be used in the visible-light photocatalytic degradation of methylene blue (MB). The catalyst had excellent performance with a degradation rate of more than 90% in a temperature span of 40 to 85 ℃. Kinetic studies showed a pseudo-first-order reaction with an extremely low activation energy at 10.78 $kJmol^{-1}$ which is a quantitative measure of a highly facile reaction pathway. Eyring analysis provided thermodynamic parameters (ΔH =8.00 $kJmol^{-1}$, ΔS = -120 J $mol^{-1}K^{-1}$) showing that a surface-mediated process with a constrained transition state occurs. The radical scavenger experiments clearly proved the presence of the superoxide radical ($O_2\bullet^-$) as the primary active species and subsumed a highly detailed charge-transfer thermodynamic reaction in which rGO transfers electrons to O_2 reduction. More importantly, the catalyst itself was found to be very stable in practice showing a 90% recovery of its starting action to perform five consecutive simple magnetic recovery cycles. Besides presenting Fe-Cu@rGO as the best photocatalyst, this study also offers some basic ideas on the synergistic functionality of this photocatalyst, which makes it a powerful photocatalyst in terms of scalable solar-based wastewater treatment.

Keywords: Photocatalysis; Methylene blue; reduced graphene oxide; bimetallic nanoparticles; Reaction mechanism; Reusability

1. Introduction

The release of industrial dye effluents, especially in the textile, printing and cosmetic sectors is a serious threat to the aquatic ecosystems and human health because these dyes are toxic, carcinogenic and non-biodegradable [1]. Methylene blue (MB) is a common example of such artificial dyes due to active photocatalytic research, as it has a stable aromatic structure and does not fade easily in water [2]. Traditional water treatment techniques like adsorption, coagulation and biological treatment are not always sufficient to fully degrade these recalcitrant organic substances, and only move pollutants onto another stage, or produce secondary waste [3, 4]. The polysaccharide-based hydrogels of natural origin has been successfully applied for the wastewater treatment, because of their stimuli-responsive, non-toxic, and chemically modifiable nature [5-25]. The photocatalysis, (particularly semiconductor-based) has become a potential green technology that can mineralize organic dyes to harmless inorganic molecules when subjected to light of specific wavelengths [26, 27].

Titanium dioxide (TiO_2) is the classical photocatalyst because of its stability, no toxicity, and high oxidizing ability [28, 29]. It however has a large bandgap (~3.2 eV), which means it only activates ultraviolet light (only 4 % of solar radiation), and it has a high rate of electron-hole recombination, which further reduces its practical efficiency. To counter these limitations, there has been a lot of research on producing visible-light-responsive catalysts and designing composite materials that have a better separation of charges [30]. It is, in this regard, that reduced graphene oxide (rGO) has received considerable interest as an ideal catalyst support due to its outstanding electrical conductivity and its high specific surface area [31], as well as its capacity to serve as an electron acceptor and transporter, and, therefore, inhibit charge recombination in semiconductor systems. Moreover, the high dispersion and stabilization of metallic nanoparticles in their two-dimensional structure and rich surface functional groups can be easily achieved [32].

Introduction of the transition metals e.g. Fe and Cu into the photocatalytic systems provides a strategic path of boosting visible-light collection and bettering interfacial charge transfer by creating heterojunctions or Schottky barriers [33, 34]. Ferrous materials, especially Fe_3O_4, add magnetic recoverability and are capable of Fenton-like reactions which generate more hydroxyl radicals [35]. Copper species, however, have been known to have narrow bandgaps and the capability to form electron traps, furthering photo response into the visible spectrum [36]. It is hypothesized that bimetallic Fe-Cu systems, based on complementary redox capabilities (Fe^{3+}, Fe^{2+} and Cu^{2+}, Cu^{3+}) to initiate long-term catalysis, may exhibit a greater benefit than their monometallic analogs based on the current available literature [37, 38].

The growth of bimetallic Fe-Cu nanoparticles on the rGO sheets with specific aim of photo catalytically degrading MB has not been fully explored even though it promises much [15, 39, 40]. A significant number of research papers are narrowed to considering single metal/rGO composites or employ expensive noble metals, and the gap in the literature lies in the development of cost-effective, efficient, and magnetically separable photocatalysts. In

addition, the interfacial charge dynamics and the predominant reactive oxygen species of such ternary systems is an evolving concept [41].

Hence, in this paper, the prepared Fe-Cu@rGO nanocomposite is critically assessed regarding its photocatalytic activity in the breakdown of MB in the visible light. It is purely application and mechanism-based as it seeks to: (i) measure the degradation performance and kinetics parameters of the catalyst at various operational temperatures [42], (ii) measure the activation energy and thermal profile of catalytic process, (iii) establish the predominant reactive oxygen species by conducting an extensive scavenger study to understand the degradation mechanism, and (iv) measure the working reusability and stability of the catalyst through a series of repeated cycles. Through this functional discussion, we will be able to develop a sound conceptualization of the dynamics that dictates the high activity of Fe-Cu@rGO, which can be useful in implementing it in future applications in the field of advanced oxidation to treat wastewater.

2. Materials and Methods

2.1. Catalyst and Chemicals

Fe-Cu@rGO, (bandgap energy of about 1.90 eV wherein the valence band potential is +1.45 eV and the conduction band potential is -0.45 eV relative to the NHE). Methylene blue, p-benzoquinone (99%), L-ascorbic acid (99%), Na_2 EDTA, (99%), and isopropanol (99.5%) were purchased at Sigma-Aldrich. Deionized water was used to prepare all solutions.

2.2. Photocatalytic Activity Assessment

The reaction rate of the photocatalytic action of Fe-Cu@rGO was tested using the process of degrading MB when subjected to visible light [44]. As a visible light source, a 300 W xenon lamp with a 420 nm cut-off filter was used. In a typical experiment, 20 mg of the catalyst was suspended in 100 mL of an aqueous solution of MB (initial concentration = 6 mg L^{-1}, initial absorbance A_0= 1.01 at λ_{max} = 664 nm) in a quartz photoreactor. The suspension was stirred in the dark using a magnet before being subjected to irradiation to attain the equilibrium of adsorption-desorption [45]. When the light was switched on, 3 mL aliquots were taken in pre-defined intervals, and the catalyst was at once separated by using an external magnet. The remaining MB concentration in the clear supernatant was then established by measuring the absorbance of its color at 664 nm in a Shimadzu UV-1800 spectrophotometer. The rate of degradation was calculated using Eq. (1):

$$\text{Degradation (\%)} = \left(1 - \frac{A_t}{A_0}\right) \times 100 \quad (1)$$

Where A_0 and A_t are the absorbances at time zero and time t respectively.

2.3. Kinetic and Thermodynamic Analysis

The pseudo-first-order model was used to study the degradation kinetics with A_0/A_t being the initial and final concentrations, respectively, and k being the apparent rate constant as in Eq. (2).

$$\ln(A_0/A_t) = kt \quad (2)$$

To determine how temperature relates to the reaction, experiments were undertaken at four temperatures (40, 55, 70, and 85 ℃) in a thermostate water bath. Arrhenius and Eyring-Polanyi plots of the temperature-dependent rate constants were used to determine the activation energy, thermodynamic parameters, enthalpy change, entropy change, and Gibbs free energy change.

2.4. Scavenger Experiments

Radical scavenger experiments were conducted to establish the prevalent reactive species that contribute to the MB degradation [46]. Separately, individual scavengers: 1 mM of p-BQ ($\bullet O_2^-$ scavenger), 1 mM of L-AA (hole scavenger), 1 mM of Na_2EDTA (hole scavenger), and 1 mM of IPA (OH• scavenger) were introduced into the solution containing the MB and then the catalyst was added and they were irradiated. The performance of the degradation at each condition at the end of 60 min of the irradiation was compared to the control experiment with no scavenger.

2.5. Catalyst Reusability and Stability Test

The efficiency of the Fe-Cu@rGO catalyst regarding practical reusability was determined by reductively repeating the photocatalytic cycles (5 cycles). The catalyst was then recovered after every cycle through a magnetic collection and then cleaned with ethanol and deionized water to eliminate any residues formed on the surface and dried overnight at 60 ℃ and reused in the same experimental conditions. The stability and longevity of the catalyst were tested by recording the degradation efficiency of every cycle [47].

3. Results and Discussion

3.1. Photocatalytic Activity and Degradation Kinetics

The photocatalytic activity of Fe-Cu@rGO in the degradation of MB with respect to irradiation of visible light at various temperatures (40, 55, 70 and 85 ℃) was conducted systematically. Figure 1 (b) shows the temporal change in efficiency of the MB degradation based on the irradiation time. There is an evident growth in degradation performance with temperature with the highest removal (approximately 75-80 %) achieved at 85 ℃ within 45 min, compared to 60-65 % at 40 ℃. This action suggests that a higher temperature favorable charge carrier movement and the reaction kinetics of the surface without thermal degradation of the catalyst.

UV-vis absorption spectra (at varying irradiation intervals) in Figure 1 (a) indicates a gradual decline in the characteristic MB absorption peak at the wavelength of about 664 nm, indicating that the chromophoric structure, rather than simple adsorption, is being destroyed.

There was also no peak shifting indicating that the degradation is primarily processed by oxidative reaction instead of by molecular aggregation or dimerization.

To quantitatively describe the degradation kinetics, the experimental data was fitted using pseudo-first-order kinetic model, which is formulated as in Eq. (3)

$$\ln(A_0/A) = kt \quad (3)$$

Figure 1 (c) demonstrates that the linear plots of $\ln(A_0/A)$ verses irradiation time were drawn at all tested temperatures, and the correlation coefficients ($R^2 > 0.98$), which confirms the suitability of the pseudo-first-order model. The rate constants (k) measured increased steadily with the temperature, which indicated that the reaction probability of the reactive oxygen species and MB molecules increased. The relatively high slope of the lines at 70 and 85 ℃ also indicate the synergetic action of Fe–Cu dual active sites and rGO conductive networks in the affinity of rapid electron transfer and inhibiting charge recombination.

3.2. Activation Energy and Arrhenius Analysis

The Kinetic rate constants were studied as a function of temperature by the Arrhenius equation:

$$\ln k = \ln A - \frac{E_a}{RT} \quad (4)$$

Figure 1 (d) shows Arrhenius plot of ln k verses 1/T giving a linear relationship with an activation energy of 10.78 kJ mol^{-1} [48]. This is a remarkably low activation energy, which explains that the photocatalytic degradation of MB in Fe-Cu@rGO is kinetically advantageous and takes place with low-energy barriers. These small Ea values are typical of highly efficient photocatalysts in which the surface redox reactions are supported by strong metal -support interactions and efficient charge separation [29]. Fe and Cu species attached to rGO probably provide a variety of redox-active sites, which allows a fast interfacial transfer of electrons. At the same time, rGO is an electron sink, which inhibits the recombination of electrons and holes and reduces the total energetic requirement of the reaction.

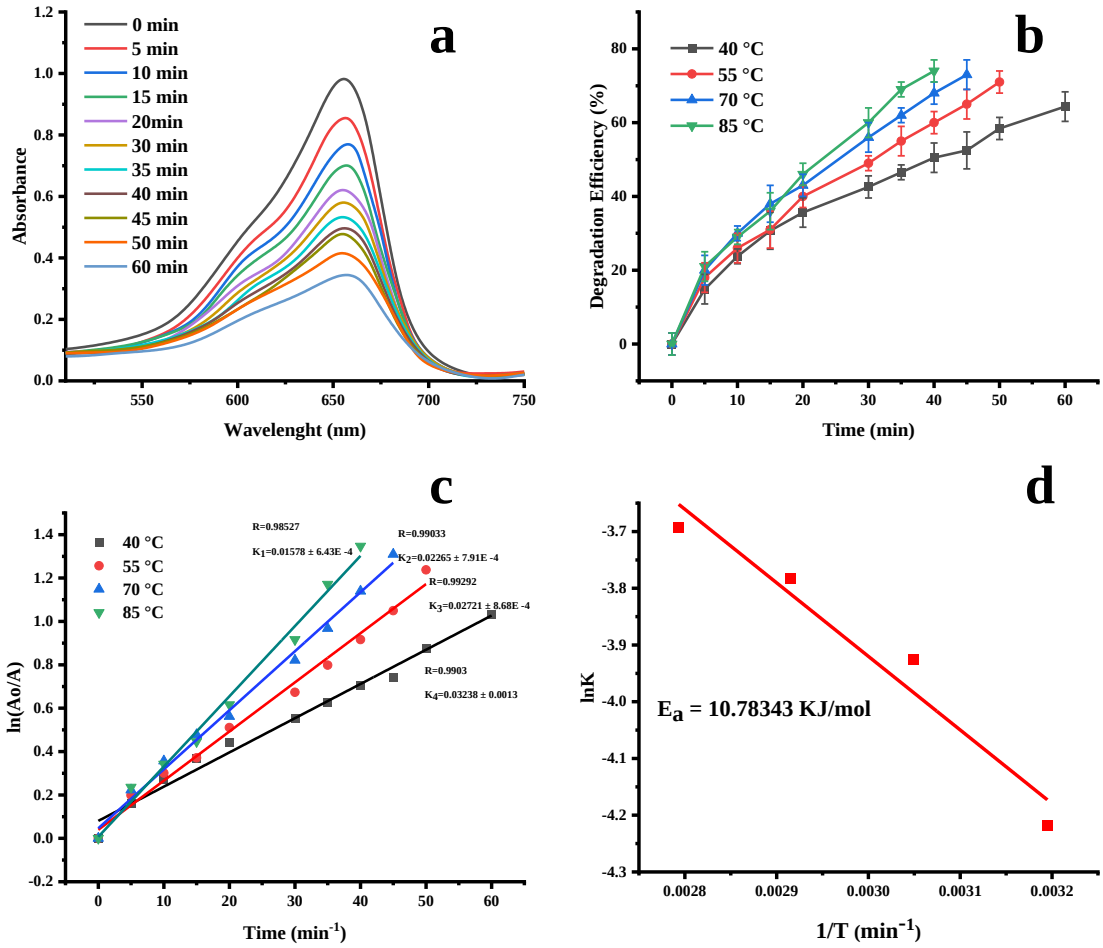

Figure 1. Photocatalytic degradation of MB dye under visible light irradiation: (a) time-dependent UV-vis absorption spectra, (b) degradation efficiency at different temperatures, (c) pseudo-first-order kinetic plots at various temperatures, and (d) Arrhenius plot for estimation of activation energy.

3.3. Thermodynamic Parameters and Reaction Feasibility

More information about the character of the photocatalytic degradation process was gained in terms of thermodynamic analysis, using Eyring equation (Figure 2 (a)). Thermodynamic parameters were calculated as represented in table 1.

Table 1. Thermodynamic parameters and activation energy for the photocatalytic degradation of MB over Fe-Cu@rGO, derived from Arrhenius and Eyring-Polanyi analyses

Thermodynamic parameters	Value	Unit
ΔH	8.00	kJ mol^{-1}
ΔS	−120	J mol^{-1} K^{-1}
ΔG	43.3	kJ mol^{-1}
Ea	10.78	kJ mol^{-1}

The fact that the change in enthalpy is positive confirms that the degradation process is endothermic, which complies with the experimentally observed increase in degradation efficiency with increasing temperature. It means that the presence of extra thermal energy promotes the creation of reactive species and promotes surface redox reactions.

The negative change in entropy implies that the amount of randomness at the solid liquid interface must decrease as the reaction proceeds, but it is possible to explain this by the fact that MB molecules and reaction intermediates are organized and adsorbed onto the Fe-Cu@rGO surface before being oxidized. This kind of ordering is usually found in heterogeneous catalytic systems that involve photocatalysis, in which reactants are absorbed as surface-bound complexes prior to mineralization. In photocatalysis, positive Gibbs free energy is not a contraindication to possible reactions, since the photo-excited charge carriers can eliminate thermodynamic constraints on the reaction, providing non-thermal energy to the system.

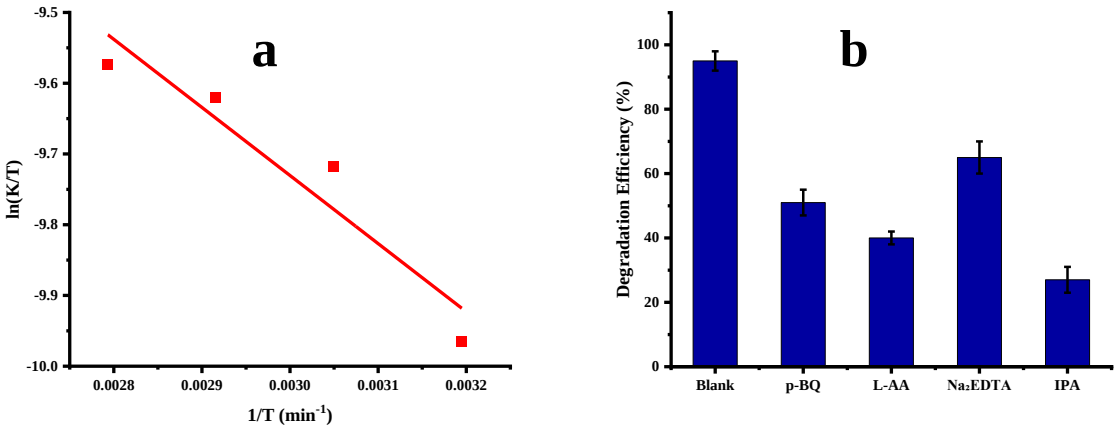

Figure 2. (a) Eyring plot for thermodynamic analysis of MB degradation over Fe-Cu@rGO, and (b) Degradation efficiency of MB dye with radical scavengers

3.4. Scavenger Studies and Proposed Degradation Mechanism

To make the transition between macroscopic performance and molecular-scale mechanism, radical scavenger experiment was performed. Figure 2 (b) shows that the dramatic quenching of the activity occurred when the p-BQ was added, and the most active species that were predominantly reactive was the superoxide radical. This crucial observation has a direct association with the conduction band electrons and their transfer to adsorbed oxygen via the rGO network as the main oxidative pathway. A strong inhibition by L-ascorbic acid and Na_2EDTA confirms the complementary role of photogenerated holes (h^+), and the small impact of isopropanol excludes a leading contribution of the free hydroxyl radicals (•OH).

When these results are combined with the characterized band positions (VB = +1.45 eV, CB = -0.45 eV vs. NHE) this gives a consistent and quantitative mechanism as shown in figure 3, whereby the following series of reactions occurs:

i. When the visible light is absorbed h^+ and e^- are excited out of the valence band and into the conduction band of the Fe-Cu active sites, leaving holes in the VB as depicted in Eq. (5).

$$\text{Fe-Cu@rGO} + h\nu \rightarrow e_{CB}^- + h_{VB}^+ \quad (5)$$

ii. Primary ROS Generation:

The electrons produced by the photogeneration quickly move to the rGO sheets that are very conductive. Electrons that are then trapped by the adsorbed molecular oxygen on the catalyst surface form the key superoxide radical as in Eq. (6).

$$e_{CB}^-(\text{via rGO}) + O_2 \rightarrow \cdot O_2^- \quad (6)$$

iii. Oxidized Forms of Hole-Mediated Pathways:

The holes that are photogenerated in the VB can be used to catalyze two parallel oxidative paths:

Direct oxidation of the adsorbed MB molecule can take place in the holes (Eq. (7)).

$$h_{VB}^+ + \text{MB} \rightarrow \text{MB}^{\cdot+} \rightarrow \text{Oxidation Products} \quad (7)$$

Indirect Oxidation: Alternatively, surface-exchange water or hydroxyl ions can react with holes to produce hydroxyl radicals although forming a secondary reaction in this system (Eq. (8-9)).

$$h_{VB}^+ + H_2O \rightarrow \cdot OH + H^+ \quad (8)$$

$$h_{VB}^+ + OH^- \rightarrow \cdot OH \quad (9)$$

iv. The reactive oxygen species (superoxide radicals, hydroxyl radicals and holes) are generated, which trigger a series of oxidative onslaughts on the MB chromophore. This causes N-demethylation, heterocyclic ring system cleavage and eventual fragmentation into smaller organic acids which eventually causes total mineralization (Eq. (10)).

$$\text{MB} + (\cdot O_2^- / \cdot OH / h^+) \rightarrow \text{Intermediates} \rightarrow CO_2 + H_2O + NO_3^- + SO_4^{2-} + \text{other ion} \qquad (10)$$

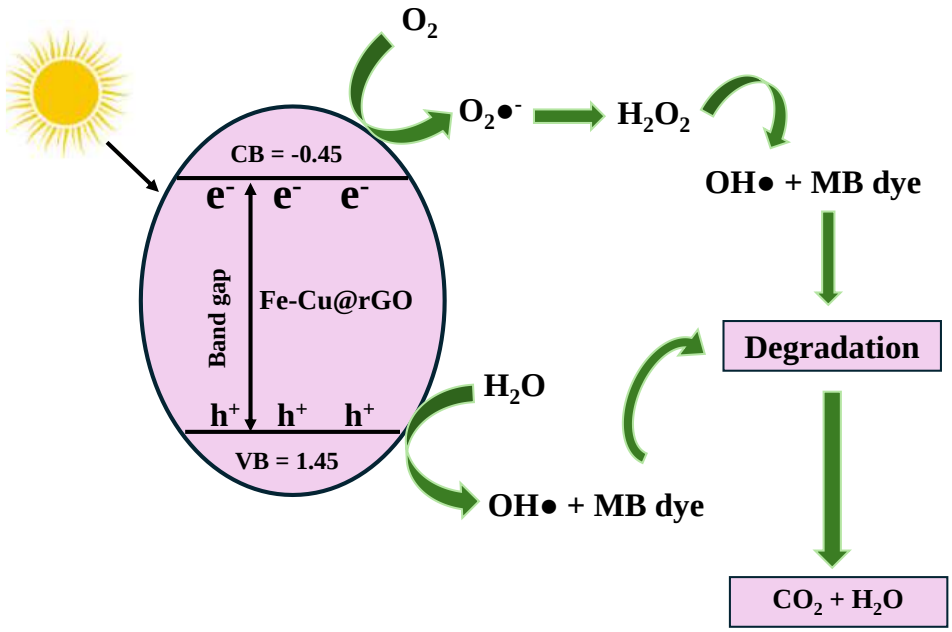

Figure 3. Mechanistic illustration of photocatalytic degradation of MB dye using Fe-Cu@rGO nanocomposite

3.5. Reusability and Stability

The stability and reusability of a photocatalyst determines the practicality and economic viability of the photocatalyst [30]. To assess this, five sequential photocatalytic cycles of Fe-Cu rGO nanocomposite at identical conditions were done with magnetic recovery and a simple washing protocol between the cycles. Figure 4 demonstrates a high level of stability in the catalyst in its operation. The efficiency of degradation of MB was always high at around 95, 93, 90, 87 and 84 % in the first to fifth cycles respectively. This is a loss of minimum activity that confirms high structural integrity of the composite. The performance retention is high due to the high anchoring of Fe-Cu nanoparticles on the rGO support to avoid the leaching and aggregation of the metal as well as the nature of rGO matrix of innate chemical stability under photocatalytic oxidative environments [29]. This excellent reusability, combined with the easy magnetic separation, highlights how the Fe-Cu@rGO catalyst has a

strong practical benefit, as it presents itself as a promising and sustainable catalyst to be reused numerous times in wastewater treatment processes.

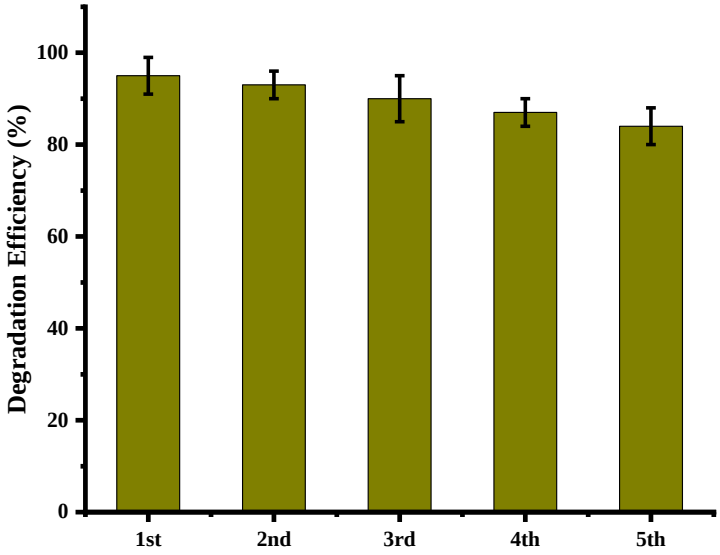

Figure 4. Reusability of the Fe-Cu@rGO catalyst over five consecutive photocatalytic cycles for MB degradation under visible light

4. Conclusion

Overall, the study offers an in-depth application and mechanistic assessment of a magnetically separable Fe-Cu@rGO nanocomposite to the efficient visible light photocatalytic degradation of MB. The high catalytic activity illustrated by the rapid degradation rate and extremely low activation energy (Ea=10.78 kJ mol^{-1}) of the catalyst is explained by the synergistic effect of the Fe-Cu bimetallic sites and the conductive support rGO. Scavenger studies by means of which the $\bullet O_2^-$ was conclusively proven to be the main oxidative species, have given rise to a hypothesis of degradation involving efficient transfer of electrons and redox reactions at the surface. More so, the composite showed excellent practical viability with a high catalytic efficiency of five reuse cycles with easy magnetic separation, a crucial problem of catalyst recovery and long-term stability. These results confirm the rational design of bimetallic-carbon hybrids is an efficient approach to the development of high-performance photocatalysts. The Fe-Cu@rGO system with its strong efficiency, explicit mechanism, with its reusability capacity holds a great future in the evolution of sustainable and solar-driven technologies to clean the organic dye contaminants in water.

References

[1] Kumari, U., 2024. Textile dyes and their impact on the natural environment. In Dye Pollution from Textile Industry: Challenges and Opportunities for Sustainable Development (pp. 17-30). Singapore: Springer Nature Singapore.

[2] Azeez, F., Al-Hetlani, E., Arafa, M., Abdelmonem, Y., Nazeer, A.A., Amin, M.O. and Madkour, M., 2018. The effect of surface charge on photocatalytic degradation of methylene blue dye using chargeable titania nanoparticles. Scientific reports, 8(1), 1-9.

[3] Koul, B., Bhat, N., Abubakar, M., Mishra, M., Arukha, A.P. and Yadav, D., 2022. Application of natural coagulants in water treatment: a sustainable alternative to chemicals. Water, 14(22), 3751.

[4] Kanwal, M., Sher, M., Abbas, A., Akhtar, S., Siddique, A.B., ul Hasan, M.N., Assad, N., Alhazmi, H.A. and Amin, H.M., 2025. Dual colorimetric sensing of Hg (II) and Fe (III) using sulfanilamide-stabilized silver nanoparticles and evaluating their photodegradation and antibacterial properties. Journal of Water Process Engineering, 75, 107981.

[5] Ali, A., Akram, A., Bakar, M.A., Amin, H.M., Zohra, L., Abbas, A., Sher, M., Hussain, M.A., Haseeb, M.T. and Imran, M., 2025. A model batch and column study for Cd (II) uptake using citric acid cross-linked *Salvia spinosa* hydrogel: Optimization through Box-Behnken design. Journal of Industrial and Engineering Chemistry, 151, 746-761.

[6] Hussain, A., Fatima, S., Abbas, A., Ali, A., Amin, M., Muhammad, G. and Sher, M., 2023. Removal of Cr (III) and Ni (II) from aqueous solution using a mixed cellulose ether-ester hydroxyethylcellulose adipate. Desalination and Water Treatment, 283, 153-163.

[7] Hussain, M.A., Gul, S., Abbas, A., Ali, A. and Alotaibi, N.F., 2021. Chemically modified rhamnogalacturonans from linseed: a supersorbent for Cd^{2+} and Pb^{2+} uptake from aqueous solution. Desalination and Water Treatment, 221, 163-175.

[8] Shehzad, M.K., Ali, A., Qasim, S., Mumtaz, A., Hussain, M.A., Fawy, K.F., Nishan, U., Azhar, I., Abbas, M.A. and Abba, A., 2025. Sustainable remediation of cadmium using succinate-functionalized glucoxylan from chia (*Salvia hispanica*) seeds hydrogel. Journal of Industrial and Engineering Chemistry. https://doi.org/10.1016/j.jiec.2025.10.034

[9] Ali, A., Haseeb, M.T., Hussain, M.A., Tulain, U.R., Muhammad, G., Azhar, I., Hussain, S.Z., Hussain, I. and Ahmad, N., 2023. A pH responsive and superporous biocomposite hydrogel of *Salvia spinosa* polysaccharide-co-methacrylic acid for intelligent drug delivery. RSC Advances, 13(8), 4932-4948.

[10] Ali, A., Hussain, M.A., Haseeb, M.T., Farid-Ul-Haq, M., Erum, A. and Hussain, M., 2024. Acute toxicity studies of methacrylic acid based composite hydrogel of *Salvia spinosa* seed mucilage: a potential non-toxic candidate for drug delivery. Cellulose Chemistry and Technology, 58(1-2), 45-53.

[11] Ali, A., Hussain, M.A., Haseeb, M.T., Tulain, U.R., Farid-ul-Haq, M., Tabassum, T., Muhammad, G., Hussain, S.Z., Hussain, I. and Erum, A., 2023. Synthesis, characterization, and acute toxicity of pH-responsive *Salvia spinosa* mucilage-co-acrylic acid hydrogel: A smart excipient for drug release applications. Reactive and Functional Polymers, 182, 105466.

[12] Ali, A., Hussain, M.A., Abbas, A., Khan, T.A., Muhammad, G., Haseeb, M.T. and Azhar, I., 2022. Comparative isoconversional thermal analysis and degradation kinetics of *Salvia spinosa* (Kanocha) seed hydrogel and its acetates: a potential matrix for sustained drug release. Cellulose Chemistry Technolog, 56(3-4), 239-250.

[13] Ali, A., Hussain, M.A., Haseeb, M.T., Ashraf, M.U., Farid-ul-Haq, M., Tabassum, T., Muhammad, G. and Abbas, A., 2023. pH-responsive, hemocompatible, and non-toxic polysaccharide-based hydrogel from seeds of *Salvia spinosa* L. for sustained release of febuxostat. Journal of the Brazilian Chemical Society, 34, 906-917.

[14] Rehman, A.U., Maqsood, A., Siddique, A.B., Akhtar, S., Fawy, K.F., Ain, Q.U., Sher, M., Nishan, U., Ahmad, T., Ali, A. and Abbas, A., 2025. From waste to water treatment: Banana peel powder for polystyrene removal with FTIR-based mechanistic understanding. Journal of Industrial and Engineering Chemistry. https://doi.org/10.1016/j.jiec.2025.11.036

[15] Ali, A., Hussain, M.A., Haseeb, M.T., Bukhari, S.N.A., Tabassum, T., Farid-ul-Haq, M. and Sheikh, F.A., 2022a. A pH-responsive, biocompatible, and non-toxic citric acid cross-linked polysaccharide-based hydrogel from *Salvia spinosa* L. offering zero-order drug release. Journal of Drug Delivery Science and Technology, 69, 103144.

[16] Amjad, F., Ali, A., Hussain, M.A., Haseeb, M.T., Ajaz, I., Farid-ul-Haq, M., Hussain, S. Z. and Hussain, I., 2025. A superabsorbent and pH-responsive copolymer-hydrogel based on glucomannans from *Ocimum basilicum* (sweet basil): A smart and non-toxic material for intelligent drug delivery. International Journal of Biological Macromolecules, 315(2), 144452.

[17] Ali, A., Haseeb, M.T., Hussain, M.A., Muhammad, T., Muhammad, G., Ahmad, N., Alotaibi, N.F., Hussain, S.Z. and Hussain, I., 2022. Extraction optimization of a superporous polysaccharide-based mucilage from *Salvia spinosa* L. Cellulose Chemistry and Technology, 56, 957-969.

[18] Iqbal, J., Kanwal, M., Siddique, A., Fawy, K.F., Sher, M., Nishan, U., ur Rehman, M.F., Abbas, M.A., Ali, A. and Abbas, A., 2025. β-Cyclodextrin-functionalized silver nanoparticles as a visual probe for selective tetrahydrocannabinol detection via host–guest induced plasmonic shifts. Microchemical Journal, 116177.

[19] Hussain, M.A., Shahzad, K., Ali, A., Haseeb, M.T. and Hussain, S.Z., 2025. Development of a novel smart bio-composite hydrogel based on dextran, citric acid, and glucoxylan for pH-dependent drug delivery and stimuli-responsive swelling and release. Polymers and Polymer Composites, 33, p.09673911251350240.

[20] Khatoon, M., Ali, A., Hussain, M.A., Haseeb, M.T., Muhammad, G., Sher, M., Hussain, S.Z., Hussain, I. and Iqbal, M., 2025. A chia (*Salvia hispanica* L.) seed mucilage-based glucoxylan-grafted-acrylic acid hydrogel: a smart material for pH-responsive drug delivery systems. Materials Advances, 6(8), 2636-2647.

[21] Hussain, M.A., Raees, N., Ali, A., Tayyab, M., Muhammd, G., Uroos, M. and Batool, M., 2025. Optimization of rhamnogalacturonan extraction from linseed using RSM and designing a pH-responsive tablet formulation for sustained release of ciprofloxacin. Cellulose Chemistry and Technology, 59, 547-558.

[22] Hussain, M.A., Taj, T., Ali, A., Haseeb, M.T., Hussain, S.Z., Muhammad, G. and Bukhari, S.N.A., 2025. Cross-Linking of Hydroxypropylcellulose With Flaxseed Rhamnogalacturonans Using Citric Acid Produces a Hemocompatible Biocomposite for pH-Responsive Rifaximin Delivery. Journal of Applied Polymer Science, e57486.

[23] Hussain, M.A., Abbas, A., Yameen, E., Ali, A., Muhammad, G., Hussain, M. and Shafiq, Z., 2022. Adsorptive removal of Pb^{2+} and Cu^{2+} from aqueous solution using an acid modified glucuronoxylan-based adsorbent. Desalination and Water Treatment, 248, 163-175.

[24] Hussain, M.A., Abbas, A., Habib, M.G., Ali, A., Farid-ul-Haq, M., Hussain, M., Shafiq, Z. and Irfan, M.I., 2021. Adsorptive removal of Ni (II) and Co (II) from aqueous solution using succinate-bonded polysaccharide isolated from Artemisia vulgaris seed mucilage. Desalination and Water Treatment, 231, 182-195.

[25] Ali, A., Hussain, M.A., Abbas, A., Haseeb, M.T., Azhar, I., Muhammad, G., Hussain, S.Z., Hussain, I. and Alotaibi, N.F., 2023. Succinylated *Salvia spinosa* hydrogel: Modification, characterization, cadmium-uptake from spiked high-hardness groundwater and statistical analysis of sorption data. Journal of Molecular Liquids, 376, 121438.

[26] Siddique, A.B., Shaheen, M.A., Abbas, A., Zaman, Y., Amin, H.M., Alam, M.M., Alharbi, N.K., Alshehri, F., Shami, A., Al-Joufi, F.A. and Ali, A., 2025. Sunlight-assisted greenly synthesised silver nanoparticles for highly selective mercury ion sensing, biomedical and photocatalytic applications. International Journal of Environmental Analytical Chemistry, 1-23.

[27] Khalid, Z., Ali, A., Siddique, A.B., Zaman, Y., Sibtain, M.F., Abbas, A., Alam, M.M. and Alwethaynani, M.S., 2025. Causonis trifolia-based green synthesis of multifunctional silver nanoparticles for dual sensing of mercury and ferric ions, photocatalysis, and biomedical applications. RSC advances, 15(21), 16879-16893.

[28] Racovita, A.D., 2022. Titanium dioxide: structure, impact, and toxicity. International Journal of Environmental Research and Public Health, 19(9), 5681.

[29] Siddique, A.B., Shaheen, M.A., Shafeeq, S., Abbas, A., Zaman, Y., Ishaque, M.Z. and Aslam, M., 2025. Optimization of photodegradation of crystal violet dye and

biomedical applications of greenly synthesized NiO nanoparticles. Materials Advances, 6(4), 1330-1344.

[30] Jiménez-Calvo, P., 2024. Synergy of visible-light responsive photocatalytic materials and device engineering for energy and environment: Minireview on hydrogen production and water decontamination. Materials Today Catalysis, 4, 100040.

[31] Tarcan, R., Todor-Boer, O., Petrovai, I., Leordean, C., Astilean, S. and Botiz, I., 2020. Reduced graphene oxide today. Journal of Materials Chemistry C, 8(4), 1198-1224.

[32] Yang, J., Zeng, Z., Kang, J., Betzler, S., Czarnik, C., Zhang, X., Ophus, C., Yu, C., Bustillo, K., Pan, M. and Qiu, J., 2019. Formation of two-dimensional transition metal oxide nanosheets with nanoparticles as intermediates. Nature Materials, 18(9), 970-976.

[33] Balapure, A., Dutta, J.R. and Ganesan, R., 2024. Recent advances in semiconductor heterojunctions: a detailed review of the fundamentals of photocatalysis, charge transfer mechanism and materials. RSC Applied Interfaces, 1(1), 43-69.

[34] Shen, L., Chen, X., Chen, Y., Peng, J., Abbas, A., Wei, J., Yu, C., Li, J. and Li, Y., 2022. One-Step Hydrothermal Synthesis of Sulfur Quantum Dots for Photoelectrochemical Catalysis for Dye Degradation. Journal of Electronic Materials, 51(6).

[35] Chen, F., Xie, S., Huang, X. and Qiu, X., 2017. Ionothermal synthesis of Fe3O4 magnetic nanoparticles as efficient heterogeneous Fenton-like catalysts for degradation of organic pollutants with H2O2. Journal of Hazardous Materials, 322, 152-162.

[36] Parveen, F., Sannakki, B., Mandke, M.V. and Pathan, H.M., 2016. Copper nanoparticles: Synthesis methods and its light harvesting performance. Solar Energy Materials and Solar Cells, 144, 371-382.

[37] Bosio, G.N., Garcia Einschlag, F.S., Carlos, L. and Mártire, D.O., 2023. Recent advances in the development of novel iron–copper bimetallic photo Fenton catalysts. Catalysts, 13(1), 159.

[38] Tang, J., Shen, L., Zhao, K., Peng, J., Chen, Q., Yu, C., Li, Y., Abbas, A., Wang, S. and Liu, Z., 2024. An ultra-sensitively ammonia-responsive gas sensor based on Ag@ sulfur nanosheets. Applied Surface Science, 643, 158574.

[39] Nguyen, T.B., Dong, C.D., Huang, C.P., Chen, C.W., Hsieh, S.L. and Hsieh, S., 2020. Fe-Cu bimetallic catalyst for the degradation of hazardous organic chemicals exemplified by methylene blue in Fenton-like reaction. Journal of Environmental Chemical Engineering, 8(5), 104139.

[40] Siddique, A.B., Shaheen, M.A., Abbas, A., Zaman, Y., Rasheed, M.U., Karim, A., Mustaqeem, M., Alam, M.M. and Alahmari, A.S., 2025. Carissa macrocarpa Extract Based Greenly Synthesized AuNPs: A Sustainable Approach for Lead Ion Detection,

Azo Dye Degradation, and Antimicrobial Applications. Water, Air, & Soil Pollution, 236(6), 1-22.

[42] Yang, B., Chen, Y. and Shi, J., 2019. Reactive oxygen species (ROS)-based nanomedicine. Chemical Reviews, 119(8), 4881-4985.

[43] Bazrafshan, E., Al-Musawi, T.J., Silva, M.F., Panahi, A.H., Havangi, M. and Mostafapur, F.K., 2019. Photocatalytic degradation of catechol using ZnO nanoparticles as catalyst: Optimizing the experimental parameters using the Box-Behnken statistical methodology and kinetic studies. Microchemical Journal, 147, 643-653.

[44] Saini, A., Madhuri, A., Sahoo, S.K., Devi, P.S., Jena, S., Laha, S. and Swain, B.P., 2024. Investigation of microstructural, chemical bonding and optical properties of Fe-Cu/rGO nanocomposites. Journal of Alloys and Metallurgical Systems, 5, 100053.

[45] Liu, H., Chen, M., Wei, D., Zhang, H., Peng, J. and Liu, G., 2020. A novel visible light controllable adsorption-desorption system with a magnetic recyclable adsorbent. Science of The Total Environment, 707, 136025.

[46] Singh, J., Chang, Y.Y., Koduru, J.R. and Yang, J.K., 2018. Potential degradation of methylene blue (MB) by nano-metallic particles: A kinetic study and possible mechanism of MB degradation. Environmental Engineering Research, 23(1), 1-9.

[47] Dai, Y., Zheng, W., Li, X., Chen, B., Wang, L. and He, G., 2016. Highly active catalysis–membrane system: Enhanced recyclability, durability and longevity properties for H2 generation. Chemical Engineering Journal, 293, 252-258.

[48] Petrou, A.L. and Economou-Eliopoulos, M., 2009. The activation energy values estimated by the Arrhenius equation as a controlling factor of platinum-group mineral formation. Geochimica et Cosmochimica Acta, 73(6), 1625-1636.

[49] Wang, P., Sheng, Y., Wang, F. and Yu, H., 2018. Synergistic effect of electron-transfer mediator and interfacial catalytic active-site for the enhanced H2-evolution performance: A case study of CdS-Au photocatalyst. Applied Catalysis B: Environmental, 220, 561-569.

[50] Kitture, R., Koppikar, S.J., Kaul-Ghanekar, R. and Kale, S.N., 2011. Catalyst efficiency, photostability and reusability study of ZnO nanoparticles in visible light for dye degradation. Journal of Physics and Chemistry of Solids, 72(1), 60-66.